

Wiley Journal of Sensors Volume 2025, Article ID 6260269, 10 pages https://doi.org/10.1155/js/6260269



Research Article

Statistical Analysis of Biased IPMC Sensor for Maximization of Sensor Sensitivity

Hojat Zamyad (1), ¹ Zahra Qaviandam (1), ¹ Nadia Naghavi (1), ¹ Alireza Shadman (1), ² and Javad Safaie (1)

¹Department of Electrical Engineering, Ferdowsi University of Mashhad, Mashhad, Iran

Correspondence should be addressed to Javad Safaie; safaie@um.ac.ir

Received 8 August 2024; Revised 9 May 2025; Accepted 6 August 2025

Academic Editor: Pramita Mishra

Copyright © 2025 Hojat Zamyad et al. Journal of Sensors published by John Wiley & Sons Ltd. This is an open access article under the terms of the Creative Commons Attribution License, which permits use, distribution and reproduction in any medium, provided the original work is properly cited.

This research aims to identify the behavioral characteristics of a biased IPMC sensor and maximize its sensitivity by optimizing the related parameters. For this purpose, an IPMC strip was stimulated with a custom setup and the experimental data was recorded. Then, a multiple linear regression model was used to determine the basic functional factors of the biased IPMC sensor. Finally, the optimal operating point of the sensor was estimated using the partial derivative method and contour plots. Statistical analysis showed that the mechanical excitation frequency, electrical bias frequency, electrical bias amplitude, and the value of bias resistance had a significant effect on the sensitivity of the IPMC sensor. Adjusted/predicted *R*-squared in the proposed model was calculated 0.9498/0.9435, respectively, which indicates high accuracy in data fitting. Also, analysis of the residuals showed that the model has the required adequacy. In addition, the consistency of the optimal operating point from the optimization method with practical experiments shows the synergy of partial derivatives and plot counters can be used as an efficient method in further optimization studies.

Keywords: biased IPMC sensor; operating point; smart materials; statistical analysis; variance analysis

1. Introduction

The IPMC sensor is a type of ion-electroactive material that has become increasingly popular as a displacement and bending sensor during the last two decades [1–9]. An IPMC sensor consists of a Nafion membrane coated with two layers of metal or other conductive materials Figure 1 [2, 10, 11]. The membrane contains an anionic lattice, hydrated cations, and water molecules that have a quite uniform distribution in rest mode (Figure 1a) [1–10], whereas bending the IPMC sensor will cause a disturbance in this ionic balance [2, 5, 6, 11]. As Figure 1b illustrates, by applying mechanical stress to the IPMC sensor, ion migration would occur due to the inside strain gradient and will then result in a potential difference between two electrode layers [2, 10, 11, 13]. As a result, any mechanical deformation in the IPMC sensor generates an

electrical signal, making it an effective displacement measurement sensor [1–10, 12].

In various studies, IPMCs have been explored for their advantages including their lightness [13], flexibility [14–16], ease of miniaturization [5], and biocompatibility [15]. However, they also have limitations, such as dependance on temperature and ambient humidity [17–21], slow dynamic response [22], hysteresis effect [23, 24], and low output voltage level [10]. Researchers have attempted to improve the performance and behavior identification of IPMC sensors through two primary optimization strategies—modifications to the fabrication process, encompassing structural, chemical, and manufacturing techniques [8, 20, 25–30], and operational protocols, incorporating electrical and environmental adjustments [31–35]—to improve sensitivity, stability, linearity, and response time.

²Department of Industrial Engineering, Ferdowsi University of Mashhad, Mashhad, Iran

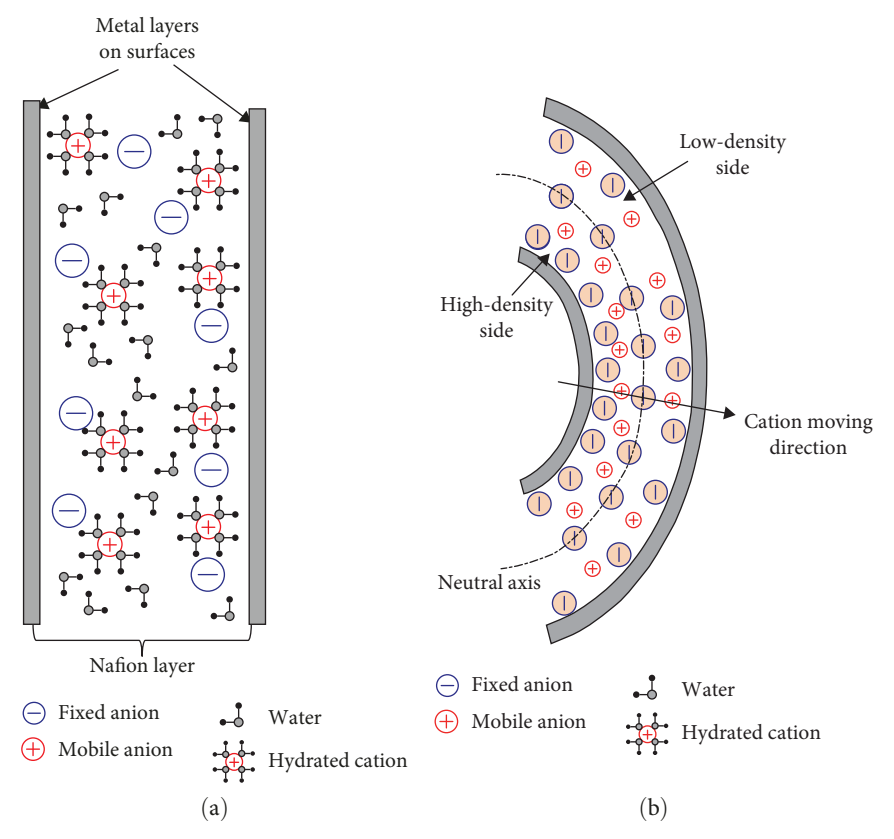


FIGURE 1: Structure and working principles of IPMC sensors [10]. (a) Rest mode and (b) sensory mode.

In the fabrication process, for structural optimization, Lee et al. [31] proposed using IPMC as a stretchable Kirigamiinspired sensor to detect strain and torsion. Their findings revealed that the Kirigami structure markedly enhances sensor sensitivity, achieving over 300% sensitivity to uniaxial strain deformation and a broad sensing range of up to 80% strain. For chemical optimization, Lee et al. [26] developed a noninvasive, intelligent throat sensor by coating the IPMC with corrosion-resistant gold. To further boost sensitivity and conformality, they engineered the Nafion membrane with a sponge-like microstructure, yielding an output with exceptional linearity and high sensitivity. Similarly, Hong et al. [36] enhanced IPMC performance by applying a conductive network composite layer of gold nanoparticles and polyallylamine hydrochloride onto the Nafion membrane, accelerating ion transport and elevating sensitivity. Likewise, Lei et al. [20] proposed coating the IPMC with an external parylene layer to mitigate drying in ambient environments, maintaining consistent water content and enabling stable sensing performance, even in dry conditions. For manufacturing optimization, Ming et al. [25] devised an innovative fluid-bed reactor for batch production of IPMC sensors, significantly improving sensitivity and stability and positioning these sensors as viable for diverse applications.

For operational protocols, in electrical optimization, Fang et al. [32] employed an amplitude modulation—demodulation technique to create an IPMC sensing/actuating transducer, where the sensor's output voltage varies with the electrical

resistance of its electrodes under bending. They explored three IPMC variants, differing in material processing and solvent conditions, and found that manufacturing variations induced deformations in static or low-frequency measurements. In environmental optimization, Andò et al. [33] placed an IPMC sensor in a small vial filled with ferrofluid to customize the behavior characteristics of IPMC. Results showed that their IPMC-based device could detect equilibrium variations, but the response of the device was limited by the output frequency of the IPMC sensor. So, through further research, Andò et al. [34] advanced this approach by leveraging external magnetic fields to control the ferrofluid environment, further refining IPMC performance. These fabrications and recording strategies support further advancements, such as our statistical analysis of biased IPMC sensors [37].

Previous studies reached some remarkable achievements, but the amplitude of the voltage generated by the IPMC sensor was still low and could be considered an obstacle; hence, through our previous study [37], a new method was introduced to improve the IPMC's performance. We applied a low amplitude high-frequency sinusoidal bias voltage signal to the IPMC, recorded its output voltage, and observed that the signal could pick up hydrated cations from stasis and facilitate their movement in the Nafion membrane, thus improving sensitivity. In this research, the influencing factors on the IPMC biased sensor and its optimal working point have been quantitatively investigated with the help of statistical methods. It is hoped that the proposed method will be a step forward in future researches in



FIGURE 2: Laboratory equipment for excitation of biased IPMC sensor and data recording.

the field of optimizing the performance of sensors based on smart materials.

2. Materials and Methods

2.1. Material. In this study, a preprepared IPMC strip with a mass of 0.17 g and dimensions of 43 mm×5 mm with a thickness of 0.5 mm was used. The electrolyte was Na⁺, and the membrane was DuPont Nafion 117 PFS, coated with two thin layers of Ag. Such IPMCs are typically prepared by cleaning the Nafion membrane in dilute acid and deionized water, followed by ion exchange with silver nitrate to impregnate Ag⁺ ions, chemical reduction to deposit Ag electrodes, and soaking in a sodium salt solution to introduce Na+ ions. Due to the influence of structural characteristics, such as length-to-width ratio and electrode-layer thickness, on IPMC behavior [8, 22], these properties are reported for validation and repeatability of experiments. According to Figure 2, the experimental setup was located in a custom incubator equipped with LM35 temperature sensor and HIH4000 hygrometer was used to maintain a constant temperature (25°C) and humidity (60%) to prevent their influence on the sensor performance. This prevented temperature and humidity from affecting the results of the experiments.

2.2. Hardware. Figure 3 presents the schematic structure of the experimental setup used in this study. The stepper motor driver circuit rotates the motor based on the given direction and frequency. Motor rotations are converted into linear motions via a mechanical coupling and bend the IPMC sensor up to 50.4° left and right of its initial position. The mechanical waveform frequency is selected proportionately to the physical limitations of IPMCs [22] and is between 0.1 and 1 Hz. Furthermore, a sinusoidal signal generator is used to provide a bias electrical wave with amplitudes of 1, 1.5, and 2 V and frequencies of 100, 200, 500, 1000, 2000, 3000, ..., and 10,000 Hz through a variable resistor named R_s (0.1, 1, and $10 \,\mathrm{k}\Omega$). The output voltage of the IPMC is recorded by a PCbased data logger (12-bit resolution, 100 kS/s sample rate in continuous streaming mode) connected to a laptop. Finally, the effect of each factor (mechanical waveform frequency, electrical bias amplitude, electrical bias frequency, and R_s value) on the output voltage (sensitivity) of IPMC is statistically analyzed. 2.3. Data Analysis. Based on previous studies, the relationship between the output voltage and tip displacement of the IPMC sensor is almost linear [9, 12, 38]. Therefore, linear models can identify key functional factors of the biased IPMC sensor. The current study provides a suitable statistical method to analyze the collected experimental data from a biased IPMC sensor. By performing appropriate statistical analysis, it is possible to identify the optimal levels of key factors to achieve the maximum output voltage and present a model for a biased IPMC sensor.

2.3.1. Multiple Linear Regression Model. In statical modeling, regression analysis is a set of statistical processes for estimating the relationships between a dependent variable and one or more independent variable(s). Generally, the multiple linear regression model is defined as follows [39]:

$$y = X\beta + \varepsilon$$

$$y = \begin{bmatrix} y_1 \\ y_2 \\ \vdots \\ y_n \end{bmatrix}, X = \begin{bmatrix} 1 & x_{11} & x_{12} & \dots & x_{1k} \\ 1 & x_{21} & x_{22} & \dots & x_{2k} \\ \vdots & \vdots & \vdots & \ddots & \vdots \\ 1 & x_{n1} & x_{n2} & \dots & x_{nk} \end{bmatrix}, \quad (1)$$

$$\beta = \begin{bmatrix} \beta_1 \\ \beta_2 \\ \vdots \\ \beta_n \end{bmatrix}, \quad \varepsilon = \begin{bmatrix} \varepsilon_1 \\ \varepsilon_2 \\ \vdots \\ \varepsilon_n \end{bmatrix}$$

where y is a vector of observed values, X is a matrix of regressors, β is the vector of estimated regression coefficients, and ε is a random error vector. Also, n represents the number of observations, and k+1 is the number of parameters of the regression model [39]. Here, the multiple linear regression is developed based on some assumptions:

- 1. A linear relationship exists between the dependent and independent variables.
- 2. The dependent variables are not highly correlated with each other.
- 3. The variance of the residuals is constant.
- 4. The observations are independent of one another.
- 5. The residuals are normally distributed.

Given such assumptions, the least-squares (LSs) method can be used as a reliable and consistent method to obtain the parameters of the regression model [40].

2.3.2. Testing the Significance of the Model and Its Parameters (Coefficients). To evaluate the significance of the regression model based on the regressors in the *X* matrix, the following hypothesis test is proposed:

$$\begin{cases} H_0: \beta_0 = \beta_1 = \dots = \beta_k = 0 \\ H_1: \exists \beta_j \neq 0 \end{cases}$$
 (2)

Here, the regression model is recognized as a statisticallysignificant model (H_0 is rejected) if at least one of the X matrix regressors is statistically significant. Variance analysis (F-test) is

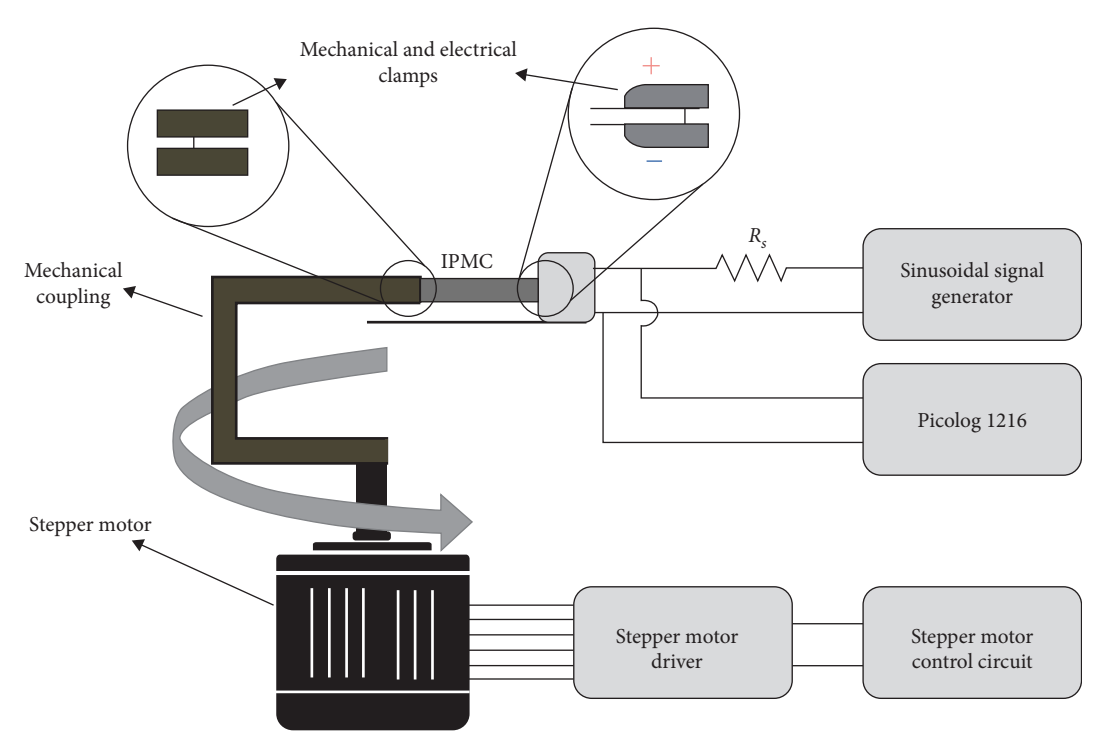


FIGURE 3: Schematic structure of the proposed hardware system for applying electrical bias and mechanical excitation to the IPMC and recording the potential difference created by it.

TABLE 1: Characteristics of tested variables.

Case	Symbol	Levels	Values	Unit
Mechanical wave frequency	f_s	3	0.1-0.4-1	Hz
Bias voltage frequency	f_b	12	0.1-0.5-1-2-3-4-5-6-7-8-9-10	kHz
Bias voltage amplitude	D_b	3	1-1.5-2	V
Variable resistance of the bias path	R_c	3	0.1-1-10	$\mathrm{k} \Omega$

used to perform this hypothesis test. In (Equation 2), the null hypothesis H_0 is rejected if $F_0 > F_\alpha$ (k, n-k-1), where α is the risk of making a type I error. According to the p-value approach, H_0 will be rejected if the p-value of the F_0 -statistic is less than α [39].

To evaluate the significance of each parameter the following hypothesis test is proposed:

$$\begin{cases} H_0: \beta_j = 0 \\ H_1: \beta_i \neq 0 \end{cases}$$
 (3)

According to the *T*-test, the hypothesis H_0 is rejected if $|t_0| > t_{\alpha/2}$ (n-k-1) and according to the *p*-value approach, H_0 will be rejected as well if the *p*-value of the t_0 -statistic is less than the α [39].

The results of tests (2) and (3) are reliable when: $\varepsilon \sim NID(0, \sigma^2)$ [39].

2.3.3. Determining the Optimal Operating Point. To determine the optimal point of a model concerning factors x_1 , x_2 , ..., x_p , partial derivatives are used. This point (if available) can be calculated from the following equation [39]:

$$\frac{\partial \widehat{y}}{\partial x_1} = \frac{\partial \widehat{y}}{\partial x_2} = \dots = \frac{\partial \widehat{y}}{\partial x_p} = 0. \tag{4}$$

In (Equation 4), \hat{y} represents the model estimation of the actual response, and the calculated operating point is called the stationary point [39]. This point can maximize or minimize the model response or be a saddle point. A contour plot is used to detect the resulting condition for the calculated operating point [39]. In addition, if it is not possible to fine-tune the stationary point in practical conditions, the contour plot helps to obtain a certain range of factor(s) for which an acceptable response is still received.

3. Result

3.1. Description of Variables. The characteristics of the tested variables (mechanical excitation frequency $[f_s]$, electrical bias frequency $[f_b]$, electrical bias amplitude $[D_b]$, and variable resistance value $[R_s]$) can be seen in Table 1. In all experiments, the amount of bending created in the IPMC was considered at \pm 50.40° (Section 2.2). So, the effect of bending amplitude is removed from the sensor response. As mentioned in Section 2.1, the ambient

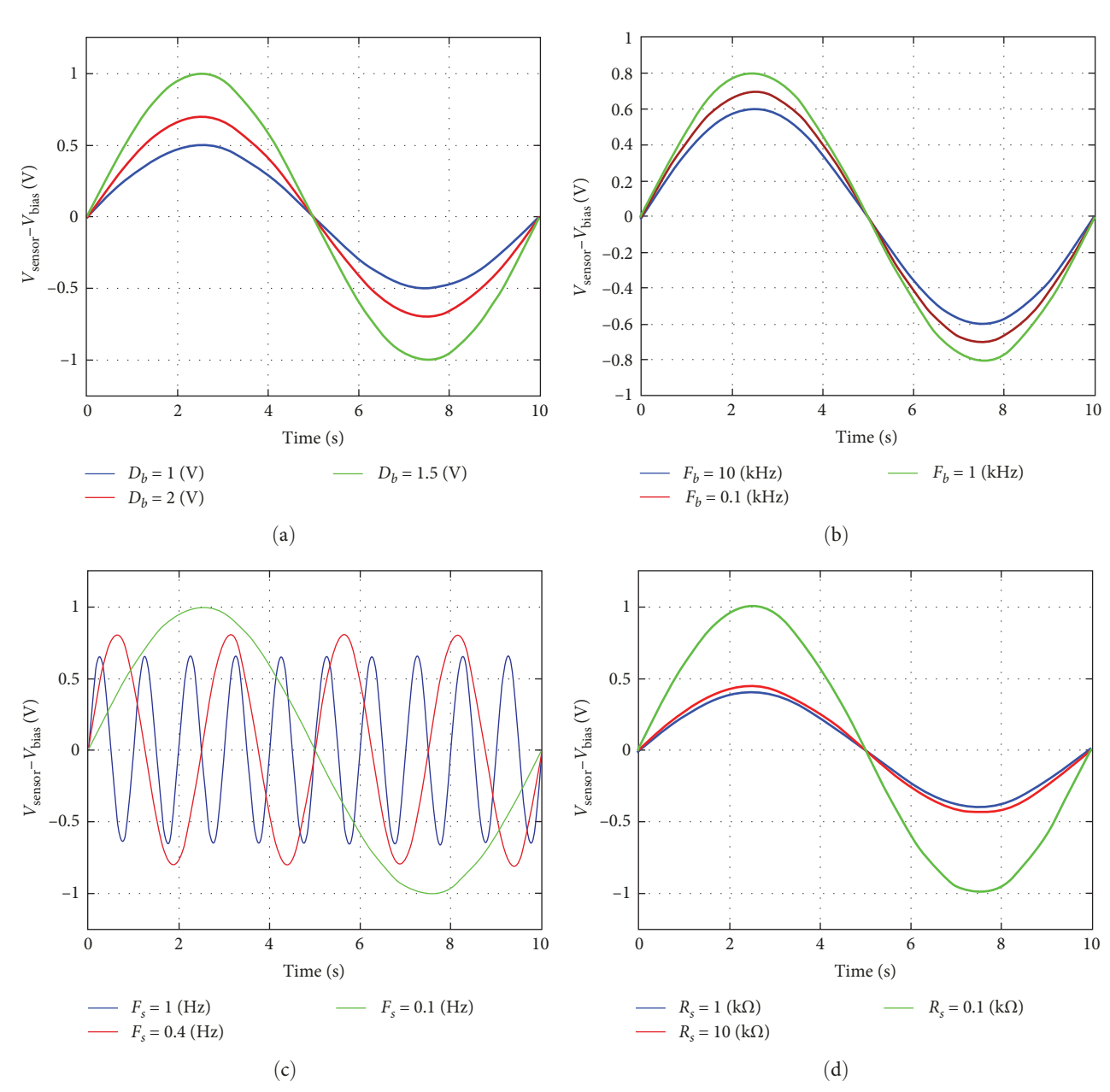


FIGURE 4: The individual effect of each parameter on the sensitivity of the biased IPMC sensor ($V_{\rm sensor-}V_{\rm bias}$). (a) The effect of bias amplitude ($f_s = 0.1 \, {\rm Hz}$, $f_b = 5 \, {\rm kHz}$, and $R_s = 1 \, {\rm k}\Omega$), (b) the effect of bias frequency ($f_s = 0.1 \, {\rm Hz}$, $D_b = 1.5 \, {\rm V}$, and $R_s = 1 \, {\rm k}\Omega$), (c) the effect of mechanical wave frequency ($D_b = 1.5 \, {\rm V}$, $f_b = 5 \, {\rm kHz}$, and $R_s = 1 \, {\rm k}\Omega$), and (d) the effect of resistance of the bias path ($f_s = 0.1 \, {\rm Hz}$, $f_b = 5 \, {\rm kHz}$, and $D_b = 1.5 \, {\rm V}$).

temperature and humidity as well as the structural parameters (aspect ratio, thickness, etc.) affect the behavior of the IPMC sensor. However, in order to avoid model complexity and focus on bias parameters, the aforementioned items have been kept constant (Section 2.1).

Figure 4 depicts the separate effect of each parameter on the sensitivity of the biased IPMC sensor. In examining each factor, other variables are held constant. The results clearly show that changing the value of each parameter affects the sensitivity of the biased sensor. Applying an electrical bias to the IPMC will result in the oscillation of the hydrated cations and facilitate their movement across the Nafion membrane. In this regard, the amplitude and frequency of the electrical bias determine the

number of hydrated cations that oscillate and their velocity of fluctuation around their position. Therefore, if the bias frequency is too high, due to the slow dynamics of the IPMC in response to electrical stimulation, the hydrated cations will not have enough time to migrate toward the cathode completely and will vibrate in the middle of the membrane. Therefore, if the bias signal frequency exceeds a certain value, the amplitude of the IPMC output voltage will drop, which is not entirely unexpected. Increment in the bias signal amplitude results in a similar outcome. This could be explained by the fact that increasing the amplitude of the bias signal is equivalent to a rise in the number of the moving hydrated cations, which, in turn, increases the probability of the collision of induced hydrated cations. During

Table 2: Analysis of variance for significance of regression related to the default model.

Source	DF	Adj SS	Adj MS	F-value	<i>p</i> -Value
Regression	12	17.9	1.492	168.07	≤0.001
Error	95	0.843	0.009	_	_
Total	107	18.743	_	_	_

Table 3: Coefficients for transformed response related to the default model.

Term	Coef	SE coef	T-value	<i>p</i> -Value
Constant	-1.764	0.288	-6.13	≤0.001
f_s	-0.565	0.165	-3.43	0.001
f_b	0.1332	0.021	6.33	≤0.001
D_b	5.743	0.361	15.93	≤0.001
R_s	0.7232	0.0438	16.52	≤0.001
$f_s \times f_s$	0.128	0.133	0.96	0.339
$f_b \times f_b$	-0.01638	0.00104	-15.79	≤0.001
$D_b \times D_b$	-1.869	0.118	-15.82	≤0.001
$R_s \times R_s$	-0.06116	0.00273	-22.37	≤0.001
$f_s \times f_b$	0.01179	0.00901	1.31	0.194
$f_s \times R_s$	-0.2347	0.0659	-3.56	0.001
$f_b \times D_b$	0.0066	0.0118	0.56	0.578
$f_b \times R_s$	0.000375	0.000918	0.41	0.684

successive collisions, the hydrated cations release their kinetic energy in the Nafion membrane and cause turbulence. Subsequently, the movement of other hydrated cations across the membrane will be disrupted. On the other hand, the output voltage drop in response to higher amplitudes of the bias signal could be related to the electrolysis phenomenon [41, 42]. Regarding the mechanical stimulation frequency, a lower frequency will bring on a higher amplitude response of the IPMC, since IPMC tip displacement with low frequencies provides hydrated cations with more time to move across the membrane. In the case of the values of R_s , inherent impedance properties of the IPMC should be noted. Therefore, the optimal value of R_s obtained from the optimization method, must have a significant relationship with the inherent impedance of IPMC.

Despite the useful information obtained from the independent examination of each parameter, statistical analysis of the results is necessary to determine the significance and contribution of each parameter to the sensor output, as well as to achieve the optimal operating point.

3.2. Determining the Optimal Regression Model. Before presenting the regression model, it is necessary to identify the regressors that have no significant effect on the response and remove them from the X matrix to minimize model complexity. A variance analysis table can be used for this purpose [39]. Considering a second-order structure as the default model, the results presented in Tables 2 and 3 were obtained. In calculating the elements of these tables, effects $D_b \times f_s$ and $D_b \times R_s$ could not be calculated and were removed. In addition, to create sufficient adequacy in the statistical model, the Box—Cox transformation

Table 4: Analysis of variance for significance of regression related to the reduced model.

Source	DF	Adj SS	Adj MS	F-value	<i>p</i> -Value
Regression	12	17.9	1.492	168.07	≤0.001
Error	95	0.843	0.009	_	_
Total	107	18.743	_	_	_

TABLE 5: Coefficients for transformed response related to the reduced model.

Term	Coef	SE coef	T-value	<i>p</i> -Value
Constant	-1.764	0.288	-6.13	≤0.001
f_s	-0.565	0.165	-3.43	0.001
f_b	0.1332	0.021	6.33	\leq 0.001
D_b	5.743	0.361	15.93	≤ 0.001
R_s	0.7232	0.0438	16.52	\leq 0.001
$f_b \times f_b$	-0.01638	0.00103	-15.87	≤0.001
$D_b \times D_b$	-1.928	0.1	-19.24	≤0.001
$R_s \times R_s$	-0.06133	0.00272	-22.58	≤ 0.001
$f_s \times R_s$	-0.2347	0.0656	-3.58	≤0.001

with a value of $\lambda = 0.25$ was applied to the response (amplitude of the voltage received from IPMC). Table 2 shows the results of the variance analysis performed to evaluate the significance of the default model. Given $\alpha = 0.05$, since $F_{0.025}$ (k, n-k-1) = 1.856 < F-value (*p*-value $< \alpha$) it is clear that the default model is significant. However, it should be noted that the removal of low-value regressors (regressors that have no significant effect on the model) reduces model complexity. According to the results presented in Table 3, the effects coefficients $f_s \times f_s$, $f_s \times$ f_b , $f_b \times D_b$, and $f_b \times R_s$ are nonsignificant due to $t_{0.025}$ (n-k-1)> |T-value| (p-value $> \alpha$). So, their regressors can be removed from the model. If these regressors are removed from the model using the backward elimination method [39], the result of the variance analysis performed to evaluate the significance of the reduced model and its effect coefficients will be as presented in Tables 4 and 5.

As can be seen in Table 4, by removing the regressors $f_s \times f_s$, $f_s \times f_b$, $f_b \times D_b$, and $f_b \times R_s$ from the model and transferring them to the error component, the degree of freedom of the model is reduced from 12 to 8. In other words, the reduced model is less complex than the default model. Also, the *F*-value of the reduced model is higher than the default model. Therefore, the reduced model is better than the default model in terms of performance.

Table 5 shows the results of the variance analysis on the reduced model coefficients. According to $t_{0.025}$ (n-k-1) = 1.984 < |T-value| $(p\text{-value} < \alpha)$, all coefficients of the reduced model are significant and should be considered in the regression model. Considering these coefficients, the reduced (optimal) regression model will be as follows:

$$\begin{aligned} \text{Voltag} e_{(\text{pk_pk})}^{0.25} &= -1.994 - 0.3644 f_s + 0.1491 f_b + 5.951 D_b \\ &+ 0.7251 R_s - 0.01638 f_b \times f_b - 1.928 D_b \times D_b \\ &- 0.06133 R_s \times R_s - 0.2347 f_s \times R_s. \end{aligned}$$

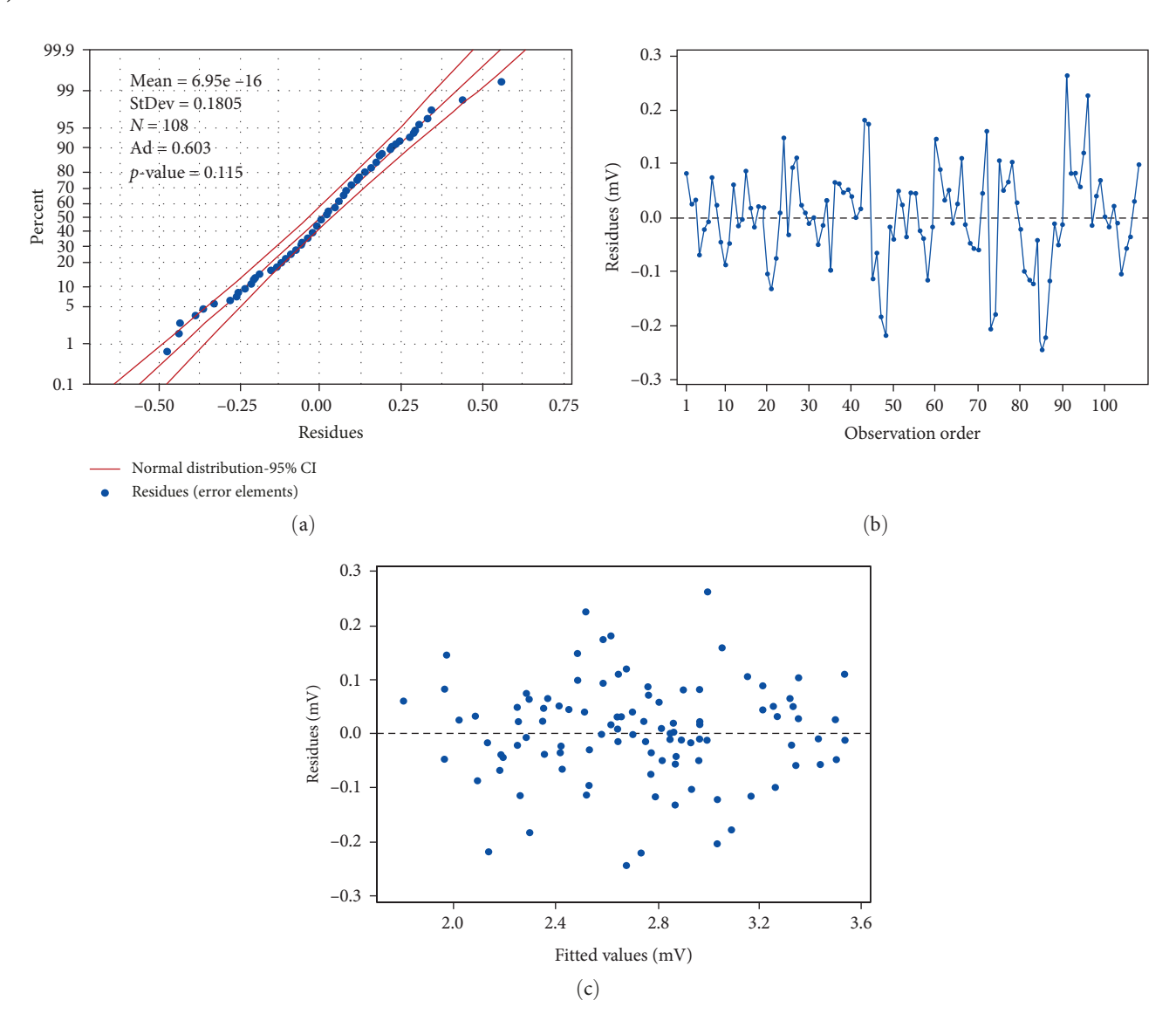


FIGURE 5: Assessing the adequacy of the regression model based on residues. (a) The comparison of residues distribution with the normal distribution. (b) The distribution of residues versus observations. (c) The trend of residues changes versus fitted values.

Based on the T-values and the reduced regression model coefficients, it is found that mechanical excitation frequency (f_s) , electrical bias frequency (f_b) , electrical bias amplitude (D_b) , and variable resistance value (R_s) are effective in the biased IPMC sensor response. Among the various effects, the amplitude of the electrical bias and the resistance of the bias path, and also their squares, play a greater role in the voltage amplitude received from IPMC, and the frequencies of the electrical bias and mechanical excitation waves are of secondary importance. Therefore, it can be said that the response of the biased IPMC sensor is resistant to changes in the frequency of bias signal and mechanical excitation, and is sensitive to changes in the amplitude of the electrical bias and the resistance of the bias path.

3.3. Validation and Adequacy of the Model. To determine the efficiency of a regression model, it is necessary to validate its performance using appropriate evaluation criteria. In this study, the adjusted coefficient of determination ($R_{\rm adjusted}^2$) and prediction coefficient of determination ($R_{\rm prediction}^2$) were used as

indicators to measure the efficiency of the model which are defined as follows [39]:

$$R_{\text{adjusted}}^2 = 1 - \frac{\frac{SS_E}{n-k-1}}{\frac{SS_T}{SS_T}},\tag{5}$$

$$R_{\text{prediction}}^2 = 1 - \frac{\text{PRESS}}{SS_T}.$$
 (6)

In (Equation 6), PRESS is the predicted residual error sum of squares and is calculated as follows [28]:

PRESS =
$$\sum_{i=1}^{n} e_{(i)}^{2} = \sum_{i=1}^{n} \left[y - \hat{y}_{(i)} \right]^{2}$$
. (7)

In (Equation 7), N-1 observation is used to calculate \hat{y} , which does not include i^{th} observation [39]. If $R_{adjusted}^2$ and

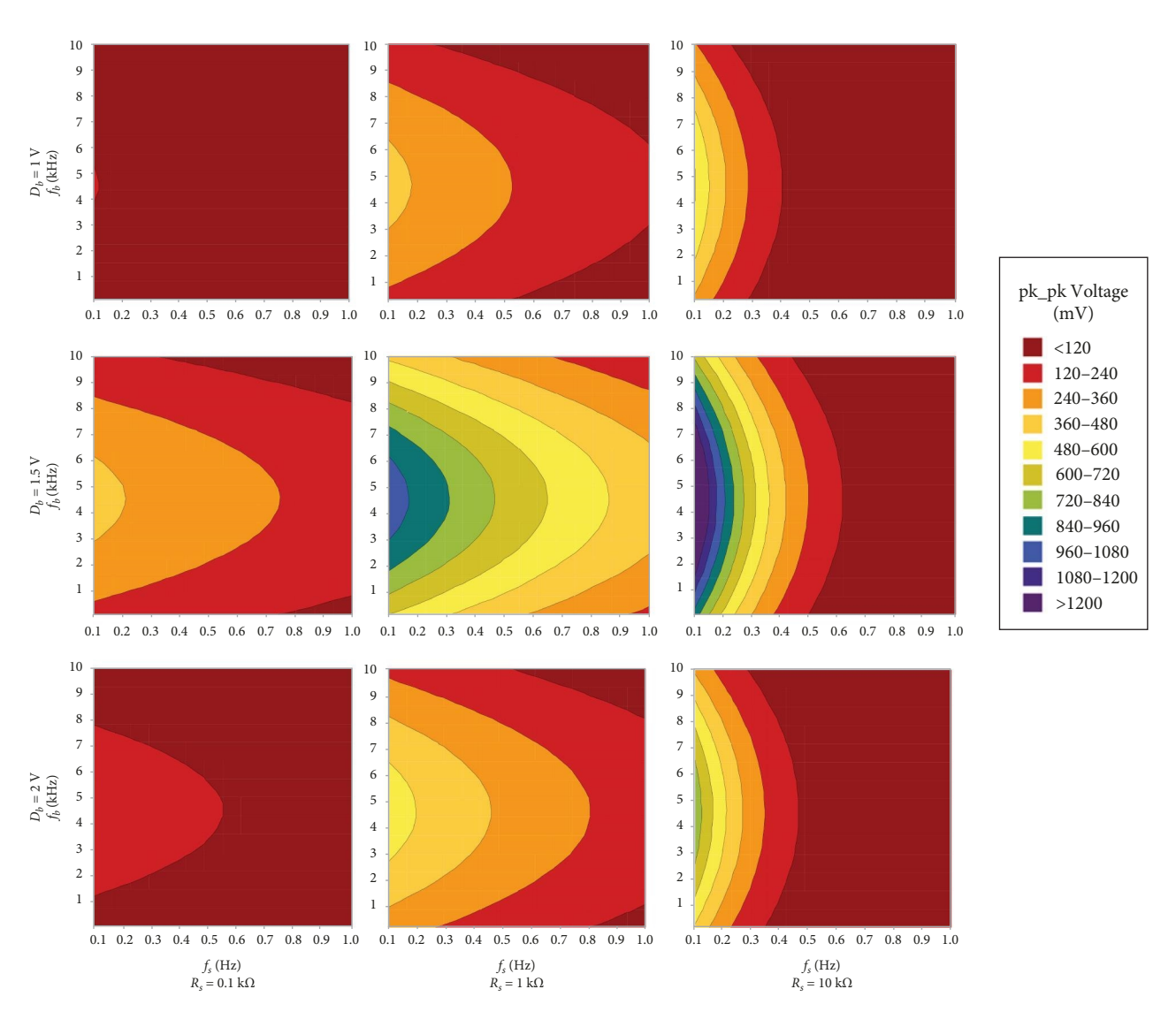


Figure 6: Contour plots of pk_pk voltage (mV) versus f_b (kHz) and f_s (Hz).

 $R_{\rm prediction}^2$ tend to one, the model will be efficient [39]. In this study, the values of $R_{\rm adjusted}^2$ and $R_{\rm prediction}^2$ were calculated as 0.9498 and 0.9435, respectively, which shows that the proposed model is highly fitted to the experimental data, and subsequent observations are also highly predictable.

Residual (error vector) analysis is a very useful approach in examining the adequacy of the modeling process [43]. The regression model is valid if the components of the error vector are normally distributed and mutually independent with zero mean and constant variance [28]. Figure 5a compares residuals distribution with normal distribution. Due to the presented results, the mean of the residuals is equal to zero and the distribution is equivalent to the normal distribution considering the 95% confidence interval (α = 0.05). Figure 5b shows the distribution of residuals versus observations (order of experiments). The presence of a random trend in this graph confirms mutually-independent error components. Furthermore, it suggests that the order of the experiments had no significant effect on the residuals. Figure 5c represents the trend of residual changes versus fitted values (regression model output). The

plot shows that errors have constant variance, with the residuals scattered randomly around zero. So, it is reasonable to assume that the error terms have a mean of zero. The vertical width of the scatter does not appear to increase or decrease across the fitted values; hence it can be assumed that the variance in the error terms is constant and the complexity considered for the regression model is quite appropriate.

3.4. Adjustment of Factors to Maximize the Output Voltage of the Biased IPMC Sensor. Figure 6 shows the contour plots of the output voltage of the biased IPMC sensor in terms of different frequencies of the mechanical stimulation, electrical bias frequencies, electrical bias amplitudes, and values of R_s . In the contour plots, the violet shading displays maximum and the red shading represents minimum voltage. Based on these plots, the optimal values of mentioned factors to obtain maximum sensitivity can be estimated approximately. Nevertheless, partial derivatives were used to obtain the accurate value of factors at the optimal operating point, according to the equation of the proposed regression model and (Equation 4). The following

output was achieved through optimization of the variables (Table 1) range:

$$f_s = 0.1(\text{Hz}), f_b = 4.6(\text{kHz}), D_b = 1.4545(\text{volt}),$$

and $R_s = 5.7(\text{k}\Omega).$

As specified by the contour plots Figure 6 and qualitative graphs of the effect of each parameter on sensor sensitivity Figure 4, it is conspicuous that this operating point is the same point of the maximum voltage response of the biased IPMC sensor.

4. Discussion and Conclusion

This study introduces a new approach to optimization of the key factional factors biased IPMC sensors' sensitivity, where a bias voltage was applied to the IPMC sensor and the amplitude of the output voltage (which was modulated over bias carrier) was recorded as the sensor response. Statistical analysis showed that the mechanical excitation frequency, electrical bias frequency, electrical bias amplitude, and the value of bias resistance have a significant effect on the amplitude of the voltage received from the biased IPMC sensor. Based on the results of statistical analysis, a regression model was proposed to predict the behavior of this sensor. Validation results showed that the proposed model had good accuracy and efficiency. Also, through the synergy of the contours and the partial derivatives method, the optimal operating point to enhance the sensitivity of the IPMC sensor was determined. It is hoped that the results of this study will play an effective role in the use of these smart materials in commercial and industrial applications and subsequent research. It should be noted that in the modeling and optimization process of this study, the effect of ambient temperature and humidity and sensor structural parameters (aspect ratio, thickness, etc.) on sensor behavior was omitted in order to focus on bias parameters. Therefore, these critical parameters should be considered in future studies.

Data Availability Statement

The data that support the findings of this study are available from the corresponding author upon reasonable request.

Ethics Statement

The authors have nothing to report.

Conflicts of Interest

The authors declare no conflicts of interest.

Author Contributions

All the authors (Hojat Zamyad, Zahra Qaviandam, Alireza Shadman, Nadia Naghavi, and Javad Safaie) actively participated in the study, experiments, analysis, and writing stages.

Funding

No funding was received for this manuscript.

References

- [1] M. Shahinpoor, Y. Bar-Cohen, J. O. Simpson, and J. Smith, "Ionic Polymer-Metal Composites (IPMCs) as Biomimetic Sensors, Actuators and Artificial Muscles-a Review," *Smart Materials and Structures* 7, no. 6 (1998): R15–R30.
- [2] M. Shahinpoor and K. J. Kim, "Ionic Polymer-Metal Composites: I. Fundamentals," *Smart Materials and Structures* 10, no. 4 (2001): 819–833.
- [3] M. Shahinpoor, "Ionic Polymer–conductor Composites as Biomimetic Sensors, Robotic Actuators and Artificial Muscles— A Review," *Electrochimica Acta* 48, no. 14–16 (2003): 2343–2353.
- [4] B. Bhandari, G.-Y. Lee, and S.-H. Ahn, "A Review on IPMC Material as Actuators and Sensors: Fabrications, Characteristics and Applications," *International Journal of Precision* Engineering and Manufacturing 13, no. 1 (2012): 141–163.
- [5] M. Hao, Y. Wang, Z. Zhu, Q. He, D. Zhu, and M. Luo, "A Compact Review of IPMC as Soft Actuator and Sensor: Current Trends, Challenges, and Potential Solutions From Our Recent Work," Frontiers in Robotics and AI 6 (2019): 129.
- [6] H. Wang, L. Yang, Y. Yang, D. Zhang, and A. Tian, "Highly Flexible, Large-Deformation Ionic Polymer Metal Composites for Artificial Muscles: Fabrication, Properties, Applications, and Prospects," *Chemical Engineering Journal* 469 (2023): 143976
- [7] Y. Wang, G. Tang, C. Zhao, et al., "Experimental Investigation on the Physical Parameters of Ionic Polymer Metal Composites Sensors for Humidity Perception," Sensors and Actuators B: Chemical 345 (2021): 130421.
- [8] P. M. Ragot, A. Hunt, L. N. Sacco, P. M. Sarro, and M. Mastrangeli, "Manufacturing Thin Ionic Polymer Metal Composite for Sensing at the Microscale," Smart Materials and Structures 32, no. 3 (2023): 035006.
- [9] S. N. Patel and S. Mukherjee, "Physics Based Modelling and Analysis of IPMC Vibration Energy Harvester," *Journal of Mechanical Science and Technology* 36, no. 8 (2022): 3983–3993.
- [10] D. N. C. Nam and K. K. Ahn, "Identification of an Ionic Polymer Metal Composite Actuator Employing Preisach Type Fuzzy NARX Model and Particle Swarm Optimization," Sensors and Actuators A: Physical 183 (2012): 105–114.
- [11] S. W. Park, S. J. Kim, S. H. Park, J. Lee, H. Kim, and M. K. Kim, "Recent Progress in Development and Applications of Ionic Polymer–Metal Composite," *Micromachines* 13, no. 8 (2022): 1290.
- [12] Q. He, G. Yin, D. Vokoun, et al., "Review on Improvement, Modeling, and Application of Ionic Polymer Metal Composite Artificial Muscle," *Journal of Bionic Engineering* 19, no. 2 (2022): 279–298.
- [13] S. J. Lee, M. J. Han, S. J. Kim, J. Y. Jho, H. Y. Lee, and Y. H. Kim, "A New Fabrication Method for IPMC Actuators and Application to Artificial Fingers," *Smart Materials and Structures* 15, no. 5 (2006): 1217–1224.
- [14] S. Guo, Y. Ge, L. Li, and S. Liu, "Underwater Swimming Micro Robot Using IPMC Actuator," in 2006 International Conference on Mechatronics and Automation, (IEEE, 2006): 249–254.
- [15] G.-Y. Lee, J.-O. Choi, M. Kim, and S.-H. Ahn, "Fabrication and Reliable Implementation of an Ionic Polymer–metal Composite (IPMC) Biaxial Bending Actuator," Smart Materials and Structures 20, no. 10 (2011): 105026.

[16] Y. Bahramzadeh and M. Shahinpoor, "Dynamic Curvature Sensing Employing Ionic-Polymer–Metal Composite Sensors," Smart Materials and Structures 20, no. 9 (2011): 094011.

- [17] P. Brunetto, L. Fortuna, P. Giannone, S. Graziani, and S. Strazzeri, "Characterization of the Temperature and Humidity Influence on Ionic Polymer–Metal Composites as Sensors," *IEEE Transactions* on *Instrumentation and Measurement* 60, no. 8 (2011): 2951– 2959.
- [18] P. Brunetto, L. Fortuna, P. Giannone, S. Graziani, and S. Strazzeri, "Static and Dynamic Characterization of the Temperature and Humidity Influence on IPMC Actuators," *IEEE Transactions on Instrumentation and Measurement* 59, no. 4 (2010): 893–908.
- [19] T. Ganley, D. L. Hung, G. Zhu, and X. Tan, "Modeling and Inverse Compensation of Temperature-Dependent Ionic Polymer–Metal Composite Sensor Dynamics," *IEEE/ASME Transactions on Mechatronics* 16, no. 1 (2011): 80–89.
- [20] H. Lei, W. Li, and X. Tan, "Encapsulation of Ionic Polymer-Metal Composite (IPMC) Sensors With Thick Parylene: Fabrication Process and Characterization Results," Sensors and Actuators A: Physical 217 (2014): 1–12.
- [21] P. Kiwon, "Characterization of the Solvent Evaporation Effect on Ionic Polymer-Metal Composite Sensors," *Journal of the Korean Physical Society* 59, no. 6 (2011): 3401–3409.
- [22] H. Zamyad and N. Naghavi, "Behavior Identification of IPMC Actuators Using Laguerre-MLP Network With Consideration of Ambient Temperature and Humidity Effects on Their Performance," *IEEE Transactions on Instrumentation and Measurement* 67, no. 11 (2018): 2723–2732.
- [23] R. Dong and Y. Tan, "A Model Based Predictive Compensation for Ionic Polymer Metal Composite Sensors for Displacement Measurement," Sensors and Actuators A: Physical 224 (2015): 43–49.
- [24] H. Zamyad, N. Naghavi, and H. Barmaki, "A Combined Fuzzy Logic and Artificial Neural Network Approach for Non-Linear Identification of IPMC Actuators With Hysteresis Modification," *Expert Systems* 35, no. 4 (2018): e12283.
- [25] Y. Ming, Y. Yang, R. P. Fu, et al., "IPMC Sensor Integrated Smart Glove for Pulse Diagnosis, Braille Recognition, and Human-Computer Interaction," Advanced Materials Technologies 3, no. 12 (2018): 1800257.
- [26] J. H. Lee, P. S. Chee, E. H. Lim, and C. H. Tan, "Artificial Intelligence-Assisted Throat Sensor Using Ionic Polymer–Metal Composite (IPMC) Material," *Polymers* 13, no. 18 (2021): 3041.
- [27] C. Bonomo, M. Bottino, P. Brunetto, et al., "Tridimensional Ionic Polymer Metal Composites: Optimization of the Manufacturing Techniques," *Smart Materials and Structures* 19, no. 5 (2010): 055002.
- [28] J. J. Pak, S. E. Cha, H. J. Ahn, and S. K. Lee, "Fabrication of Ionic Polymer Metal Composites by Electroless Plating of Pt," in In 32nd International Symposium on Robotics and 1st Intelligent Microsystem Symposium (2001): 291–295
- [29] H. Lei, W. Li, G. Zhu, and X. Tan, "Evaluation of Encapsulated Ipmc Sensor Based on Thick Parylene Coating," in *In ASME* 2012 Conference on Smart Materials, Adaptive Structures and Intelligent Systems, (American Society of Mechanical Engineers, 2012): 35–42.
- [30] G.-H. Feng and R.-H. Chen, "Improved Cost-Effective Fabrication of Arbitrarily Shaped µIPMC Transducers," *Journal of Micro*mechanics and Microengineering 18, no. 1 (2008): 015016.
- [31] J.-H. Lee, P.-S. Chee, E.-H. Lim, J.-H. Low, and N.-T. Nguyen, "A Stretchable Kirigami-Inspired Self-Powered Electroactive Sensor for Tensile Strain and Torsion Sensing," *Advanced Engineering Materials* 24, no. 4 (2022): 2100961.

- [32] B.-K. Fang, C.-C. K. Lin, and M.-S. Ju, "Development of Sensing/Actuating Ionic Polymer–Metal Composite (IPMC) for Active Guide-Wire System," *Sensors and Actuators A: Physical* 158, no. 1 (2010): 1–9.
- [33] B. Andò, C. Bonomo, L. Fortuna, et al., "A Bio-Inspired Device to Detect Equilibrium Variations Using IPMCs and Ferrofluids," *Sensors and Actuators A: Physical* 144, no. 2 (2008): 242–250.
- [34] B. Andò, S. Baglio, A. Beninato, S. Graziani, F. Pagano, and E. Umana, "A Seismic Sensor Based on IPMC Combined With Ferrofluids," *IEEE Transactions on Instrumentation and Measurement* 62, no. 5 (2013): 1292–1298.
- [35] D. J. Griffiths, "Development of Ionic Polymer Metallic Composites as Sensors (Doctoral Dissertation Virginia Tech)," (2008).
- [36] W. Hong, A. Almomani, and R. Montazami, "Electrochemical and Morphological Studies Of Ionic Polymer Metal Composites. as Stress Sensors," *Measurement* 95 (2017): 128–134.
- [37] Z. Qaviandam, N. Naghavi, and J. Safaie, "A New Approach to Improve IPMC Performance for Sensing Dynamic Deflection: Sensor Biasing," *IEEE Sensors Journal* 20, no. 15 (2020): 8614–8622.
- [38] I. Dominik, J. Kwaśniewski, and F. Kaszuba, "Ionic Polymer-Metal Composite Displacement Sensors," *Sensors and Actuators A: Physical* 240 (2016): 10–16.
- [39] D. C. Montgomery, Design and Analysis of Experiments (John Wiley & Sons, 2017).
- [40] L. Ljung, "System Identification," in Signal Analysis and Prediction, (1998): 163–173.
- [41] Y. Bar-Cohen, S. P. Leary, A. Yavrouian, et al., "Challenges to the Application of IPMC as Actuators of Planetary Mechanisms," in Smart Structures and Materials 2000: Electroactive Polymer Actuators and Devices (EAPAD), 3987, (International Society for Optics and Photonics, 2000): 140– 147.
- [42] J.-W. Lee and Y.-T. Yoo, "Anion Effects in Imidazolium Ionic Liquids on the Performance of IPMCs," *Sensors and Actuators B: Chemical* 137, no. 2 (2009): 539–546.
- [43] H. Zamyad, S. Sahebian, and J. Safaie, "Behavior Identification of Silicone-Ethanol Soft Actuator Based on Statistical Analysis," Advanced Theory and Simulations 8, no. 5 (2025): 2401388.